High Mitochondrial Respiration and Glycolytic Capacity Represent a Metabolic Phenotype of Human Tolerogenic Dendritic Cells

This information is current as of August 9, 2022.

Frano Malinarich, Kaibo Duan, Raudhah Abdull Hamid, Au Bijin, Wu Xue Lin, Michael Poidinger, Anna-Marie Fairhurst and John E. Connolly

Supplementary Material	http://www.jimmunol.org/content/suppl/2015/04/25/jimmunol.1303316.DCSupplemental
References	This article **cites 35 articles**, 12 of which you can access for free at: http://www.jimmunol.org/content/194/11/5174.full#ref-list-1

Why *The JI*? Submit online.

- **Rapid Reviews! 30 days*** from submission to initial decision

- **No Triage!** Every submission reviewed by practicing scientists

- **Fast Publication!** 4 weeks from acceptance to publication

*average

Subscription	Information about subscribing to *The Journal of Immunology* is online at: http://jimmunol.org/subscription
Permissions	Submit copyright permission requests at: http://www.aai.org/About/Publications/JI/copyright.html
Email Alerts	Receive free email-alerts when new articles cite this article. Sign up at: http://jimmunol.org/alerts

High Mitochondrial Respiration and Glycolytic Capacity Represent a Metabolic Phenotype of Human Tolerogenic Dendritic Cells

Frano Malinarich,*,† Kaibo Duan,† Raudhah Abdull Hamid,*,† Au Bijin,*,† Wu Xue Lin,*,† Michael Poidinger,† Anna-Marie Fairhurst,† and John E. Connolly*,†,‡

Human dendritic cells (DCs) regulate the balance between immunity and tolerance through selective activation by environmental and pathogen-derived triggers. To characterize the rapid changes that occur during this process, we analyzed the underlying metabolic activity across a spectrum of functional DC activation states, from immunogenic to tolerogenic. We found that in contrast to the pronounced proinflammatory program of mature DCs, tolerogenic DCs displayed a markedly augmented catabolic pathway, related to oxidative phosphorylation, fatty acid metabolism, and glycolysis. Functionally, tolerogenic DCs demonstrated the highest mitochondrial oxidative activity, production of reactive oxygen species, superoxide, and increased spare respiratory capacity. Furthermore, assembled, electron transport chain complexes were significantly more abundant in tolerogenic DCs. At the level of glycolysis, tolerogenic and mature DCs showed similar glycolytic rates, but glycolytic capacity and reserve were more pronounced in tolerogenic DCs. The enhanced glycolytic reserve and respiratory capacity observed in these DCs were reflected in a higher metabolic plasticity to maintain intracellular ATP content. Interestingly, tolerogenic and mature DCs manifested substantially different expression of proteins involved in the fatty acid oxidation (FAO) pathway, and FAO activity was significantly higher in tolerogenic DCs. Inhibition of FAO prevented the function of tolerogenic DCs and partially restored T cell stimulatory capacity, demonstrating their dependence on this pathway. Overall, tolerogenic DCs show metabolic signatures of increased oxidative phosphorylation programing, a shift in redox state, and high plasticity for metabolic adaptation. These observations point to a mechanism for rapid genome-wide reprograming by modulation of underlying cellular metabolism during DC differentiation. *The Journal of Immunology*, 2015, 194: 5174–5186.

D endritic cell (DC) maturation status plays a key role in regulating the balance between immunity and tolerance (1, 2). DC maturation is a tightly coordinated response involving multiple signaling pathways, molecular trafficking, cytokine production, and cytoskeletal remodeling (3–5). These processes require energetic metabolic adaptations important for DC survival, migration, and ultimately the development of pathogen-specific immunity. Understanding the metabolic changes underpinning DC immune function could help develop new strategies for controlling immunogenicity. Studies in mice have demonstrated that T cell activation and differentiation from naive into effector and memory T cells are processes highly dependent on energetic metabolic adaptations. This knowledge is currently being considered for potential novel immune therapies (6–8). However, knowledge surrounding the immune-metabolic states of DCs is rather limited.

Maturation of murine bone marrow–derived DCs (BMDCs) is highly dependent on metabolic changes. In the immature state, oxidative phosphorylation (OXPHOS) and fatty acid oxidation (FAO) are the main energy sources. DC maturation coincides with an increase in mitochondrial OXPHOS followed by a pronounced switch to aerobic glycolysis (9–11). Importantly, pharmacological inhibition of glycolysis prevents BMDC maturation, suggesting the importance of this metabolic switch for DC immunogenicity (10, 11).

Consistent with the studies in mice, downregulation of OXPHOS gene expression has been reported during human monocyte-derived DC (moDC) maturation (12). In contrast to mature moDCs, proteomic analysis of tolerogenic moDCs, which are resistant to maturation (13), has shown a predominance of OXPHOS pathway proteins (14). Therefore, a comparative analysis across the spectrum of moDCs is required to explain the metabolic changes between immunogenic and tolerogenic moDC states.

In this study, we compared the changes in energetic metabolism among human moDCs. Protein expression and functional analyses

*Institute of Molecular and Cell Biology, Agency for Science, Technology and Research, Singapore 138673; †Singapore Immunology Network, Singapore 138648; and ‡Institute of Biomedical Studies, Baylor University, Waco, TX 76798

Address correspondence and reprint requests to Dr. John E. Connolly, Institute of Molecular and Cell Biology, 61 Biopolis Drive, Proteos, Room 7-17B, Singapore 138673. E-mail address: jeconnolly@imcb.a-star.edu.sg

The online version of this article contains supplemental material.

Abbreviations used in this article: ACADM, acyl-CoA dehydrogenase, C-4 to C-12 straight chain; BMDC, bone marrow–derived DC; CM-H$_2$DCFDA, 5-(and-6)-chloromethyl-2′,7′-dichlorodihydrofluorescein diacetate, acetyl ester; COXII, cyclooxygenase II; DC, dendritic cell; DEG, differentially expressed gene; 2-DG, 2-deoxy-D-glucose; ECAR, extracellular acidification rate; FAO, fatty acid oxidation; FCCP, carbonyl cyanide 4-(trifluoromethoxy)phenylhydrazone; HADHA, hydroxyacyl-CoA dehydrogenase/3-ketoacyl-CoA thiolase/enoyl-CoA hydratase, α subunit; HADHB, hydroxyacyl-CoA dehydrogenase/3-ketoacyl-CoA thiolase/enoyl-CoA hydratase, β subunit; iNOS, inducible NO synthase; IPA, ingenuity pathway analysis; LDHB, lactate dehydrogenase B; moDC, monocyte-derived DC; OCR, oxygen consumption rate; OXPHOS, oxidative phosphorylation; ROS, reactive oxygen species; SO, superoxide; SRC, spare respiratory capacity.

demonstrated that tolerogenic moDCs have a prominent and stable OXPHOS program with high reactive oxygen species (ROS) and superoxide (SO) production, as well as a robust mitochondrial spare respiratory capacity (SRC). Although tolerogenic and immature moDCs displayed similar levels of FAO activity, glycolytic capacity, and reserve, these catabolic pathways were maintained at a low level in mature moDCs. Finally, tolerogenic moDCs, in contrast to mature moDCs, demonstrate a high bioenergetic plasticity for metabolic adaptation in terms of ATP production.

Materials and Methods

moDC generation

Monocytes were purified from PBMCs of healthy donors (Institutional Review Board approval NUS-IRB 10-250) by density centrifugation (Ficoll–Paque, GE Healthcare), followed by magnetic separation (CD14 MicroBeads, Miltenyi Biotec) (purity >92%) and cultured in complete medium (RPMI 1640 with 10% FBS, 100 U/ml penicillin, 100 μg/ml streptomycin, 1 mM pyruvate, 2 mM L-glutamine, nonessential amino acids, 15 mM HEPES, and 50 μM 2-ME) in presence of GM-CSF and IL-4 (both 1000 U/ml, Miltenyi Biotec). At days 4 and 6, cells were refreshed with cytokines. To obtain tolerogenic moDCs, cells were treated at day 5 with 10 nM dexamethasone and 100 nM vitamin D_3 (Sigma-Aldrich). Cells were then either treated with LPS (*Escherichia coli* O128-B12, 1 μg/ml, Sigma-Aldrich) at day 6 or left untreated. At day 7, immature (untreated), mature (LPS-treated), tolerogenic, and LPS-tolerogenic moDCs were harvested and washed for further experiments. For experiments addressing the effect of metabolic modulators on tolerogenicity/immunogenicity of moDCs, day 6 tolerogenic and immature moDCs were treated with either etomoxir (10 μM), oxamate (50 mM), 2-deoxy-D-glucose (2-DG; 50 mM), or oligomycin (2 μM) followed by stimulation with LPS (1 μg/ml). Twenty-four hours later, at day 7, metabolically modulated LPS-tolerogenic and mature moDCs were harvested and washed for further experiments.

Alloreaction studies

CD4+ T cells were purified from allogeneic PBMCs by magnetic separation (StemCell Technologies) and labeled with 5 μM CellTrace CFSE (Molecular Probes). CFSE-labeled CD4+ T cells were cultured in 96-well U-bottom plates with 0–40 × 10^3 moDCs for 6 d for proliferation analysis. For analysis of early markers of T cell activation, $2.0 × 10^5$ CD4+ T cells were cultured in 96-well U-bottom plates with 0–40 × 10^3 moDCs for 24 h and analyzed by flow cytometry.

Flow cytometry

moDC phenotypic analysis was performed using anti–CD80-PE (L307.4), anti–CD83-PE (HB15e), anti–CD86-PE (IT2.2), and anti–CD11c-allophycocyanin (S-HCL-3) (BD Biosciences); anti–HLA-DR-PerCP (L243) (BioLegend); anti–CD141-PE (BDCA1, AD5-14H12), anti–CD1c-PE (BDCA3, AD5-8E7), and anti–CD14-FITC (TÜK4) (Miltenyi Biotec); and anti-ILT3 (ZM4.1) (eBioscience). DAPI staining was used for live/dead cell discrimination. Day 6 alloreactive CFSE-labeled CD4+ T cells were stained with anti–CD3-PerCP (UCHT1) and anti–CD4-PE-Cy7 (RPA-T4) (BioLegend) and with anti–CD25-allophycocyanin-Cy7 (M-A251) (BD Biosciences). Dead cells were discriminated by trypan blue Live/Dead staining (Molecular Probes). Intracellular Foxp3 detection was assessed using Cytofix/Cytoperm kit (BD Biosciences) with the Foxp3–Alexa Fluor 647 Ab (259D/C7, BD Biosciences). Early activation status of alloreactive CD4+ T cells was assessed using the following Ab mixture: anti–CD69-PerCP (L78, BD Biosciences), anti–CD4-PE-Cy7 (RPA-T4, BioLegend), and anti–CD3-PE (OKT3, eBioscience).

Mitochondria membrane potential, ROS, and SO were determined after moDC labeling with 100 nM Red CMXRos, 5 μM 5-(and-6)-chloromethyl-2′,7′-dichlorodihydrofluorescein diacetate, acetyl ester (CM-H_2DCFDA), and 5 μM MitoSOX (Molecular Probes), respectively, in HBSS for 30 min at 37°C. All flow cytometry data were acquired on FACSCanto II and LSR II (BD Biosciences) and analyzed using FlowJo v.9.5 (Tree Star).

Cytokine and protein analysis

Supernatants from alloreactions were collected for cytokine profiling by multiplex analysis using a human cytokine/chemokine bead panel (Milliplex Map, Millipore). The levels of OXPHOS, FAO, and glycolytic protein content were measured from moDC lysates using human OXPHOS magnetic bead panel, human FAO panel 1/2, and human glycolysis pathway panel kits (Millipore), respectively, using a FLEXMAP 3D system (Luminex).

Mitochondrial DNA content determination

Total DNA from moDCs was isolated by phenol-chloroform extraction as previously described (15). Real-time PCR was performed in the Stratagene Mx3005P quantitative PCR system using the SYBR Green/ROX FAST Mastermix kit (Qiagen) with GAPDH (forward, 5′-CCTAGGGCTGCT-CACATATTC-3′, reverse: 5′-CGCCCAATACGACCAAATCTA-3′) and cyclooxygenase II (COXII; forward: 5′-GTTGTAGCCCACTTCCAC-TATG, reverse: TAGGGTGTAGCCTGAGAATAGG-3′) primers. The mitochondrial/nuclear DNA content was calculated by using the formula: $2^{-CT\ mitochondrial\ COXII}/2^{-CT\ nuclear\ GAPDH}$. Data were analyzed by MxPro quantitative PCR software (Agilent Technologies).

Real-time metabolic characterization

The mitochondria oxygen consumption rate (OCR, O_2 mpH/min) and extracellular acidification rate (ECAR, mpH/min) of moDCs were analyzed by an XF^{e}96 extracellular flux analyzer (Seahorse Bioscience). For OCR studies, moDCs were harvested, washed, and resuspended in OCR medium (DMEM base, 25 mM glucose, 1 mM pyruvate, 2 mM L-glutamine [pH 7.35]). Cells (60 × 10^3/well) were plated in poly-D-lysine–coated 96-well flat-bottom plates and incubated in a non-CO_2 incubator for 1 h at 37°C. A complete OCR study was performed with all moDC types simultaneously in four consecutive stages: basal respiration (without drugs), mitochondrial complex V inhibition (2 μM oligomycin), maximal respiration induction [0.5 μM carbonyl cyanide 4-(trifluoromethoxy)phenylhydrazone (FCCP)], and electron transportation chain inhibition (1 μM rotenone and 1 μM antimycin A). FAO studies included an additional stage immediately after basal respiration (100 μM etomoxir, FAO inhibition). The percentage of FAO activity (FAO index) was assessed as [(basal − etomoxir respiration)/(basal − olygomycin respiration)] × 100. For ECAR analysis, moDCs were harvested, washed, and resuspended in ECAR medium (DMEM base [no bicarbonate] with 2 mM L-glutamine, 143 mM NaCl, and 0.5% phenol red [pH 7.35]), and the complete ECAR analysis consisted of four stages: basal (without drugs), glycolysis induction (10 mM glucose), maximal glycolysis induction (2 μM oligomycin), and glycolysis inhibition (100 mM 2-DG).

ATP content determinations

For intracellular ATP measurements, 20 × 10^3/well moDCs in OCR medium were incubated for 75 min at 37°C in the presence or absence of 2 μM oligomycin, 100 μM etomoxir, and 100 mM 2-DG. ATP levels were determined with CellTiter-Glo luminescent cell viability assay (Promega). In parallel, a viability assay was performed with 1 μM calcein AM (Molecular Probes) in HBSS for 30 min at 37°C and the percentage of viable cells was assessed by comparing the level of fluorescence emission of drug-treated and untreated cells. Digitonin-treated moDCs were used as positive control for dead cells.

Fatty acid and glucose uptake

The uptake of fatty acids was studied using a free fatty acid uptake assay fluorometric kit (Abcam). moDCs (1 × 10^5/well) were resuspended in HBSS and incubated for 30 min at 37°C in CO_2 incubator, followed by the addition of the fluorescent fatty acid probe. After 1 h of incubation, fluorescence levels were determined (excitation 485 nm, emission 530 nm) in the fluorescence microplate reader SpectraMax Gemini EM (Molecular Devices).

For glucose uptake analysis, moDCs were resuspended in DMEM glucose-free medium and incubated for 90 min at 37°C in CO_2 incubator with 30 μM 2-(N-(7-nitrobenz-2-oxa-1,3-diazol-4-yl)amino)-2-deoxyglucose (Molecular Probes). Finally, moDCs were stained with DAPI, washed, and the glucose uptake levels were measured by flow cytometry in the FITC channel.

Lactate and NO production

Lactate levels were analyzed from moDCs culture supernatants at day 7 using the colorimetric L-Lactate assay kit (Abcam), according to the manufacturer's protocol. For the determination of glycolytic capacity, 2 x 10^4 moDCs/well in ECAR medium were incubated for 75 min at 37°C in the presence or absence of 10 mM of glucose or 2 μM oligomycin. Lactate levels were measured from supernatants using the fluorometric L-Lactate assay kit (Abcam).

NO production was measured as nitrite from moDCs culture supernatants using the colorimetric NO assay kit (Abcam), according to the manufacturer's protocol.

Microarray and bioinformatic data analysis

Total RNA of 16 samples from four moDC types (tolerogenic, LPS-tolerogenic, immature, and mature) were extracted by TRIzol (Invitrogen) followed by a clean-up procedure using an RNeasy micro kit (Qiagen). All RNA samples had an integrity number ≥9.6 assessed by an Agilent Bioanalyzer. Total RNA samples were amplified using TargetAmp, and the biotinilated cRNA was prepared by Nano-g biotin-aRNA labeling kit for the Illumina system (Epicentre Biotechnologies). After the hybridization to the Illumina human HT-12 v4 BeadChips for 17 h at 58°C, the arrays were washed, stained (Illumina wash protocol), and then scanned using BeadArray scanner 500GX. Array data were extracted at the probe level without background correction using Illumina GenomeStudio software. These raw data were quantile normalized and $\log_2$ transformed. Technical replicates were obtained from the hybridization in duplicate of three samples. Pearson correlation analysis showed high correlation between the technical replicates ($r > 0.99$). Differentially expressed genes (DEGs) were identified using Limma (16) with Benjamini–Hochberg multiple testing correction ($p < 0.05$). DEGs were further clustered into different groups according to the patterns of expression change among the different moDC types using STEM software. The analysis was performed in R v.2.12.2 (http://www.R-project.org) with Bioconductor 2.12 (http://www.bioconductor.org) and enabled by Pipeline Pilot (http://www.accelrys.com). Metabolic/signaling pathway analyses of DEGs were done by ingenuity pathway analysis (IPA; Ingenuity Systems, http://www.ingenuity.com). Microarray data have been deposited at National Center for Biotechnology Information, Gene Expression Omnibus (GEO), accession no. GSE52894 (http://www.ncbi.nlm.nih.gov/geo/query/acc.cgi?token=arwhicsyrnchxmb&acc=GSE52894).

Statistical analysis

Significant differences between multiple comparisons were determined using one-way or two-way ANOVA with Tukey or Dunnett posttests, with a p value <0.05 considered significant. Analysis was completed using Prism 6 (GraphPad Software).

Results

Tolerogenic moDCs exhibit a distinctly high metabolic energy signature

Donor-matched untreated (immature), LPS-treated (mature), and dexamethasone/vitamin D_3–treated (tolerogenic) moDCs were analyzed for their respective immunological functional traits. Tolerogenic moDCs were additionally stimulated with LPS (LPS-tolerogenic moDCs) to verify resistance to maturation (13). Analysis of DC surface marker expression showed that HLA-DR (MHC class II), CD83, and CD86 expression levels in tolerogenic moDCs were similar to immature moDCs. Furthermore, tolerogenic moDCs exhibited a resistance to maturation following LPS stimulation, compared with mature moDCs, which had high expression for all three markers (Supplemental Figs. 1A, *upper panel*, 2A). All moDCs expressed similar levels of CD11c. However, tolerogenic and LPS-tolerogenic moDCs showed increased expression of CD14, BDCA3, and ILT3 compared with immature or mature moDCs, consistent with previous reports (17) (Supplemental Fig. 1A, *lower panel*). Functional analyses demonstrated that tolerogenic moDCs were poorly immunogenic, as shown by low alloproliferation of CD4 T cells (Supplemental Fig. 1B) as well as low IFN-γ, low IL-12p40, and high IL-10 cytokine production in cocultures compared with mature moDCs (Supplemental Fig. 1C). Furthermore, tolerogenic moDCs actively suppressed alloproliferation induced by mature moDCs. Additionally, tolerogenic moDCs increased the frequency of CD25^{high}Foxp3$^+$ regulatory T cells (Supplemental Figs. 1D, 2) and inhibited IFN-γ production while increasing IL-10 cytokine production (Supplemental Fig. 1E). This inhibition of allogeneic T cell proliferation was functionally dominant because it could not be overcome with the addition of mature moDCs (Supplemental Fig. 1F).

Having established a phenotypically and functionally defined model of tolerogenic moDCs, we performed a transcriptomic study

to identify energetic metabolism "signatures" in each of the moDCs. This analysis revealed a DEG pattern for tolerogenic moDCs relative to the other moDCs (Fig. 1A, *left panel*). IPA showed that this tolerogenic moDC-specific DEG profile was enriched for pathways involved in energy metabolism, including the citrate cycle, OXPHOS, mitochondria dysfunction, pyruvate metabolism, glycolysis/gluconeogenesis, mTOR and HIF1α signaling, and fatty acid metabolism (Fig. 1A, *right panel*). The individual DEGs for each metabolic pathway highly expressed only in tolerogenic moDCs are shown in Table I.

Because we observed that immature, tolerogenic, and LPS-tolerogenic moDCs were poorly immunogenic (Supplemental Fig. 1A–C), we analyzed the DEGs highly expressed for these moDC types compared with mature moDCs (Fig. 1B, *left panel*). The IPA of this profile was similar to the tolerogenic moDC DEG profile described above (Fig. 1B, *right panel*). The individual DEGs for each metabolic pathway highly expressed on tolerogenic, LPS-tolerogenic, and immature moDCs are shown in Table II. In contrast, IPA of DEGs highly expressed only in mature moDCs (Fig. 1C, *left panel*) revealed no enrichment for energetic metabolism pathways, with the exception of the mTOR and AMPK signaling pathways (Fig. 1C, *right panel*). Moreover, DEGs expressed by mature moDCs were found to be enriched for pathways involved in lymphotoxin β receptor and TNFR signaling, together with DC maturation pathways (Fig. 1C, *right panel*). The individual DEGs for each pathway highly expressed only in mature moDCs are shown in Table III.

In conclusion, tolerogenic, LPS-tolerogenic, and immature moDCs highly express genes involved in energetic metabolism. These include genes in glycolytic and mitochondrial catabolic pathways. In contrast, mature moDCs exhibit a pronounced proinflammatory gene signature.

Tolerogenic moDCs highly express genes and proteins of OXPHOS

Because our data had indicated an upregulation in mitochondrial energetic metabolism pathways, we then examined the phenotypic differences between tolerogenic and immunogenic moDCs. Transcriptome analyses confirmed that many of the genes in the OXPHOS pathway were highly expressed in tolerogenic moDCs, including members of complexes I–V (Fig. 2A). These are important components of the electron transport chain and O_2-coupled ATP synthesis. Most of these genes were downregulated following LPS exposure, particularly in mature moDCs (Fig. 2A).

Protein analysis of the OXPHOS pathway demonstrated that LPS significantly decreased complex I levels (Fig. 2B). Importantly, tolerogenic and LPS-tolerogenic moDCs had higher levels of complexes II to IV compared with immature and mature moDCs. Finally, the content of complex V was not significantly different among moDCs (Fig. 2B).

In summary, these data demonstrate that tolerogenic moDCs exhibit a high expression of OXPHOS complex I to V genes. Additionally, LPS negatively regulate these genes, irrespective of tolerogenic activity. In contrast to the transcript levels, tolerogenic moDCs express high levels of assembled OXPHOS complexes, with only the protein content of complex I negatively affected by LPS.

Tolerogenic moDCs exhibit high mitochondrial functional activity

Our data demonstrated that tolerogenic moDCs have higher content of proteins involved in the OXPHOS pathway, indicating the potential for a higher mitochondrial activity. To confirm that these metabolic phenotypes impacted function, we analyzed the mito-
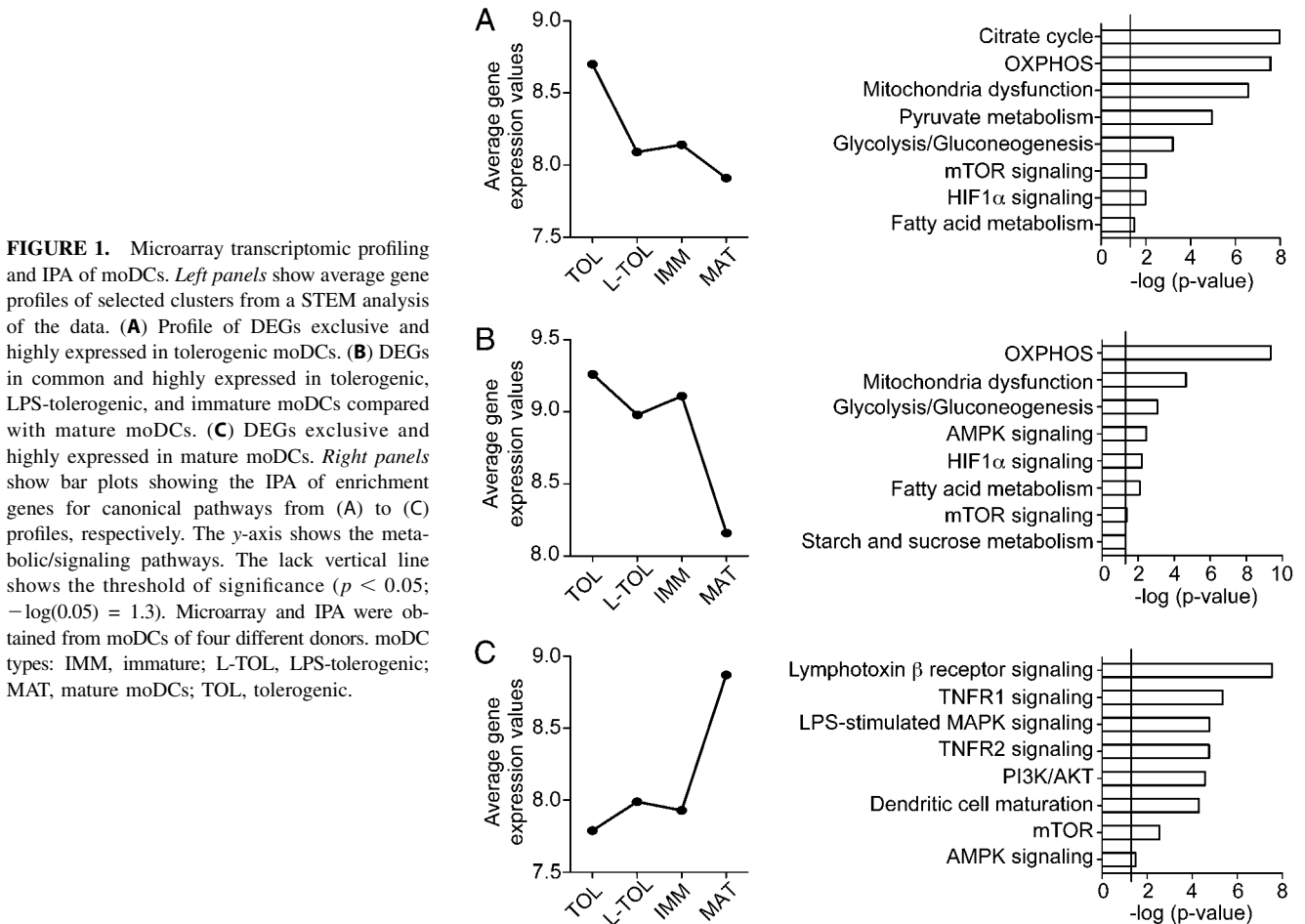
FIGURE 1. Microarray transcriptomic profiling and IPA of moDCs. *Left panels* show average gene profiles of selected clusters from a STEM analysis of the data. (**A**) Profile of DEGs exclusive and highly expressed in tolerogenic moDCs. (**B**) DEGs in common and highly expressed in tolerogenic, LPS-tolerogenic, and immature moDCs compared with mature moDCs. (**C**) DEGs exclusive and highly expressed in mature moDCs. *Right panels* show bar plots showing the IPA of enrichment genes for canonical pathways from (A) to (C) profiles, respectively. The *y*-axis shows the metabolic/signaling pathways. The lack vertical line shows the threshold of significance ($p < 0.05$; $-\log(0.05) = 1.3$). Microarray and IPA were obtained from moDCs of four different donors. moDC types: IMM, immature; L-TOL, LPS-tolerogenic; MAT, mature moDCs; TOL, tolerogenic.

chondrial membrane potential levels, reflecting the mitochondrial activity, in moDCs using MitoTracker (Red CMXRos). Analyses showed that tolerogenic moDCs have higher mitochondrial activity compared with the other moDC types. Furthermore, LPS did not suppress this increased mitochondrial activity (Fig. 3A). Because mitochondrial activity is an important source of ROS, particularly SO, we analyzed baseline activity using CM-H$_2$DCFDA and MitoSOX, respectively. We found that tolerogenic moDCs produced greater levels of ROS compared with immature and mature moDCs (Fig. 3B). Similarly, tolerogenic moDCs demonstrated the highest capacity for SO generation, followed by immature moDCs, LPS-tolerogenic moDCs, and finally mature moDCs, which had the lowest capacity to produce SO (Fig. 3C). Given

these observations, we hypothesized that moDCs might have different OXPHOS activity levels in terms of mitochondrial O$_2$ consumption. We therefore examined the OCR of all moDCs in real time using a Seahorse bioanalyzer, as depicted in Fig. 3D. We observed high levels of basal and maximal respiration following FCCP addition in tolerogenic moDC cultures (Fig. 3E). Quantitative analysis confirmed that tolerogenic moDCs had higher basal OCR levels compared with mature moDCs (Fig. 3F, *upper panel*). Furthermore, tolerogenic, LPS-tolerogenic, and immature moDCs had increased SRC compared with mature moDCs (Fig. 3F, *lower panel*). Because it has been recognized that TLR-induced NO production causes the block in mitochondrial respiration in murine BMDCs (9), we examined the NO production levels from moDC

Table I. IPA of DEGs highly expressed only in tolerogenic moDCs

Metabolic Pathway	$-\text{Log}$ (p Value)	DEGs
Citrate cycle	7.98	*SDHA, PCK2, SUCLG2, SUCLG1, ACO2, IDH3A, MDH2, ACO1, IDH3B*
OXPHOS	7.58	*SDHA, ATP5J, COX7A2, ATP5O, COX6A1, UQCR11, UQCRB, NDUFS1, UQCR10, NDUFB9, COX11, NDUFS8, CYC1, UQCRC1, ATP5G3*
Mitochondrial dysfunction	6.58	*SDHA, ATP5J, COX7A2, COX6A1, UQCRB, PDHA1, NDUFS1, NDUFB9, PRDX3, COX11, NDUFS8, CYC1, UQCRC1, SNCA*
Pyruvate metabolism	4.95	*PKM2, PDHA1, ALDH2, PCK2, ME3, ACSS1, ME1, MDH2, LDHB*
Glycolysis/gluconeogenesis	3.21	*PKM2, PDHA1, ALDH2, DHRS9, GAPDH, ACSS1, TPI1, LDHB*
mTOR signaling	2.00	*EIF3B, EIF4A3, PIK3R1, RPS19, RPS21, RPS6KA2, RPS6KA1, EIF3C/EIF3CL, RPS12*
HIF1a signaling	1.98	*SLC2A5, TP53, SLC2A1, PIK3R1, NOS3, TCEB1, LDHB*
Fatty acid metabolism	1.49	*ALDH2, SLC27A5, DHRS9, ACADVL, ACOX2, ACADM*

Table II. IPA of DEGs highly expressed in tolerogenic, LPS-tolerogenic, and immature moDCs

Metabolic Pathway	−Log (p Value)	DEGs
OXPHOS	9.36	SDHB, COX7B, ATP5D, COX8A, NDUFB5, ATP5L, NDUFB6, NDUFA8, COX6B1, LHPP, NDUFV3, UQCR10, ATP5h, ATP5B, NDUFA6, NDUFA12, NDUFA3, COX15
Mitochondrial dysfunction	4.66	COX6B1, COX7B, GLRX2, NDUFV3, NDUFB5, COX8A, TRAK1, BACE1, PSENEN, SDHB, GSR, ATP5B, NDUFA6, NDUFA12, NDUFB6, NDUFA3, COX15, NDUFA8, PINK1
Glycolysis/gluconeogenesis	3.07	PKM2, HK1, GPI, DHRS9, ALDH3A2, GAPDH, FBP1, ALDOA, HK3, ALDH9A1, ALDH7A1, DHRS4
AMPK signaling	2.47	CHRNB4, EIF4EBP1, KAT2B, MTOR, MAPK14, PPP2R3A, PIK3R6, MRAS, PRKAR1B, PPM1A, MAP2K3, MLYCD, PPAT, ATM, ADRB2
HIF1a signaling	2.21	EGLN1, MAPK14, COPS5, PIK3R6, MRAS, NAA10, TCEB1, APEX1, PDGFC, SLC2A3, P4HTM, ATM
Fatty acid metabolism	1.83	HADHB, DHRS9, ALDH3A2, ECI2, ACSL5, ACAD8, ALDH9A1, HADHA, CYP1B1, ALDH7A1, DHRS4
mTOR signaling	1.36	RPS6KA3, EIF3E, PDGFC, EIF3M, EIF4EBP1, MTOR, RHOT1, PPP2R3A, EIF4A1, PIK3R6, MRAS, RPS6KA2, PRKD3, PRKCB, ATM
Starch and sucrose metabolism	1.32	HK1, GPI, UGDH, HPSE, HK3, MTAP, GBA2

supernatants. Surprisingly, tolerogenic moDCs and mature moDCs showed similar production of NO levels (Fig. 3G). Interestingly, tolerogenic moDCs also showed higher mitochondrial content than did immature and mature moDCs. This increase in tolerogenic moDCs was not affected by LPS treatment (Fig. 3H).

In summary, we have found increased mitochondrial content and OXPHOS activity (ROS production and O_2 respiration) in tolerogenic moDCs, which showed stable mitochondrial function despite stimulation with LPS. Furthermore, these data suggest that NO production alone was not sufficient to account for the observed decrease in mitochondrial activity in terms of ROS production, basal respiration, and SRC induced by LPS.

OXPHOS in tolerogenic moDCs utilizes mitochondrial FAO activity

The enhanced mitochondrial activity observed in tolerogenic moDCs might require FAO as an energy source for OXPHOS

maintenance (18). Transcriptome analysis of moDC types revealed a higher expression of distinctive cluster FAO-associated genes in tolerogenic and immature moDCs compared with mature moDCs (Fig. 4A). Protein analysis confirmed the upregulation of four components involved in fatty acid catabolism: acyl-CoA dehydrogenase, C-4 to C-12 straight chain (ACADM), hydroxyacyl-CoA dehydrogenase/3-ketoacyl-CoA thiolase/enoyl-CoA hydratase, α and β subunits (HADHA/HADHB, mitochondrial trifunctional protein), and carnitine palmitoyltransferase 2 in tolerogenic moDCs. In contrast, mature moDCs have the highest level of L-bifunctional enzyme (EHHADH), which is involved in the peroxisomal β-oxidation pathway (Fig. 4B). FAO enzymes that were not significantly different between tolerogenic and mature moDCs are listed in Supplemental Fig. 3A. Importantly, because mitochondrial FAO is linked with O_2 consumption for OXPHOS (19), we studied the relative contribution of FAO to OXPHOS by monitoring mitochondrial OCR changes in moDCs using a Seahorse bioanalyzer.

Table III. IPA of DEGs highly expressed only in mature moDCs

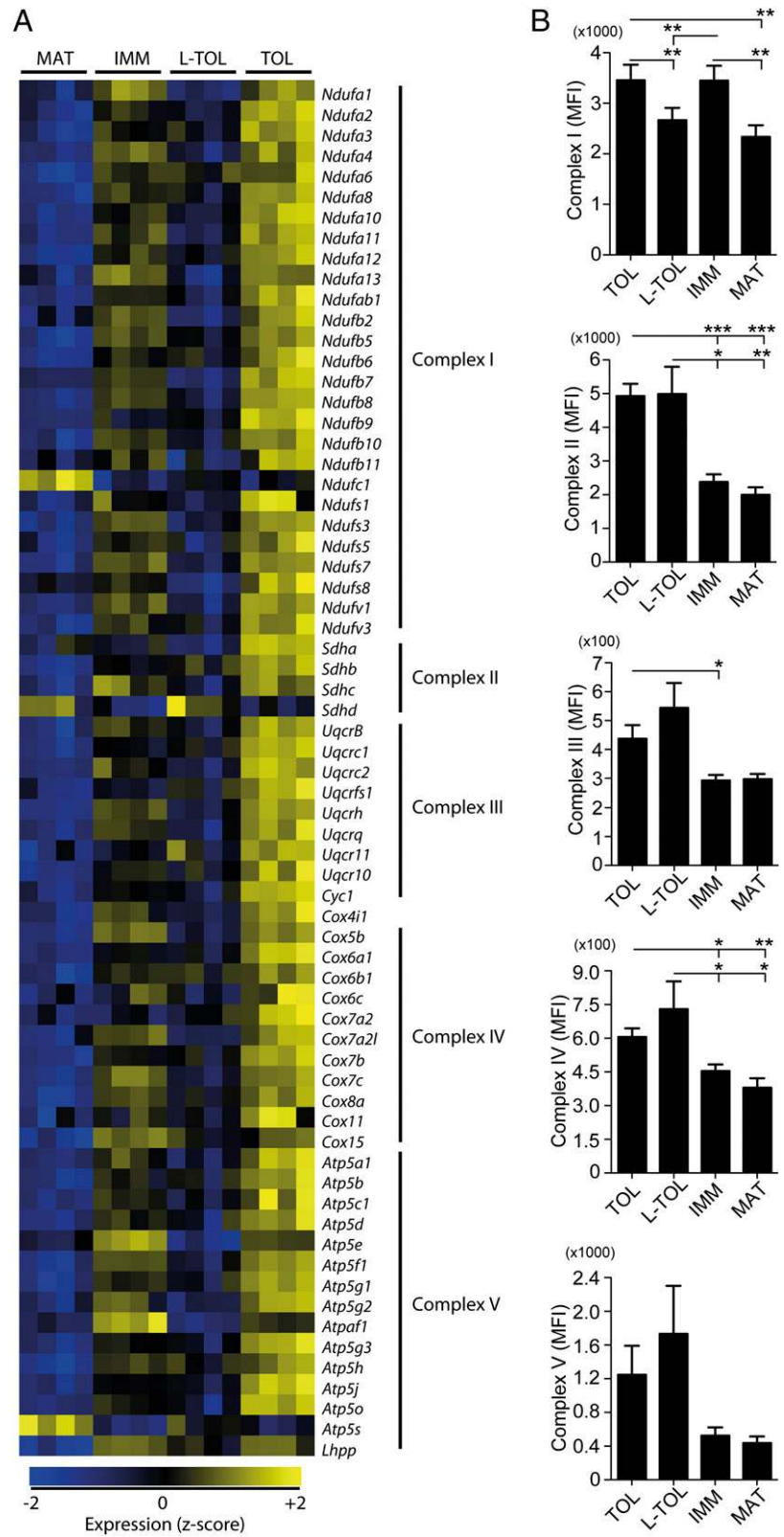| Metabolic Pathway	−Log (p Value)	DEGs
Lymphotoxin β receptor signaling	7.55	MAP3K14, PIK3C2B, PIK3CA, MAPK1, CASP3, RELB, CREBBP, PIK3R5, NFKB2, TRAF6, NFKBID, BCL2L1, IKBKG, TRAF2, CASP9, LTA, BIRC2, TRAF1
TNFR1 signaling	5.35	MAP3K14, CASP3, MAP3K1, NFKB2, FADD, TANK, TRADD, TRAF2, IKBKG, CASP9, BIRC3, CASP7, BIRC2
LPS-stimulated MAPK signaling	4.76	MAP3K14, PIK3C2B, PIK3CA, NRAS, MAPK1, RAC1, PIK3R5, HRAS, NFKB2, MAPK11, PRKCZ, ATF2, IKBKG, PRKCD, CREB1, PRKD1
TNFR2 signaling	4.75	TANK, MAP3K14, TRAF2, IKBKG, LTA, MAP3K1, NFKB2, BIRC3, BIRC2, TRAF1
PI3K/AKT signaling	4.58	PIK3CA, NRAS, JAK1, MAPK1, PPP2R5D, ILK, YWHAZ, HRAS, NFKB2, PRKCZ, BCL2L1, PPP2CB, IKBKG, FOXO1, PPP2R4, PPP2R3A, CDKN1A, CTNNB1, PPP2R1B, ITGA4
DC maturation	4.30	PIK3CA, MAPK1, PIK3R5, CD83, MAPK11, IKBKG, CREB1, LY75, TAB1, PIK3C2B, MAP3K14, RELB, CREB3, IL15, CD58, NFKB2, DDR1, ATF2, TRAF6, IL12B, LTA, FSCN1, HLA-DOB, CD86, CCR7
mTOR signaling	2.56	PIK3C2B, PLD2, PIK3CA, NRAS, MAPK1, PRKAB1, PPP2R5D, PIK3R5, RAC1, HRAS, RPS27L, PRKCZ, PPP2CB, RHOV, PPP2R4, PPP2R3A, PRKCD, RPS6KA5, RHOF, PPP2R1B, FNBP1, AKT1S1, PRKD1
AMPK signaling	1.50	PIK3C2B, PIK3CA, MAPK1, PRKAB1, AK8, CPT1B, PPP2R5D, CHRNB1, PIK3R5, MAPK11, PPP2CB, PPM1B, PPP2R4, PPP2R3A, PPP2R1B

FIGURE 2. Gene and OXPHOS protein complexes content in moDCs. (**A**) Heat map representing gene expression levels of OXPHOS complexes in all moDC types (IMM, immature; L-TOL, LPS-tolerogenic; MAT, mature; TOL, tolerogenic). Heat map shows gene level z-score–normalized gene expression levels of moDCs from four different donors. (**B**) Protein levels of electron transport chain complex I, II, III, IV, and ATP synthase complex V in all moDC types. The data were pooled from six independent experiments. Mean ± SEM. Statistical differences were analyzed by one-way ANOVA with a Tukey multiple comparison posttest. $*p < 0.05$, $**p < 0.01$, $***p < 0.001$.

The FAO inhibitor etomoxir decreased the OCR and maximal respiration in all moDCs, with the greatest effect being observed on tolerogenic and immature moDCs, with a less pronounced effect on LPS-tolerogenic moDCs and the least in mature moDCs (Fig. 4C). From these experiments, we calculated the FAO index, which is the ratio between OCR changes induced by etomoxir relative to oligomycin. Tolerogenic and immature moDCs had the highest FAO index, which decreased following LPS treatment (Fig. 4D). We have also observed that etomoxir-treated mature moDCs showed similar SRC compared with untreated mature moDC. This further suggests a low contribution of FAO to energetic metabolism in mature moDCs (Fig. 4C). Despite the differences observed in their mitochondrial FAO levels, all moDC types presented similar ability of fatty acid uptake (Fig. 4E). In conclusion, both tolerogenic and immature moDCs express a specific set of FAO genes with different enzymatic content than that of mature
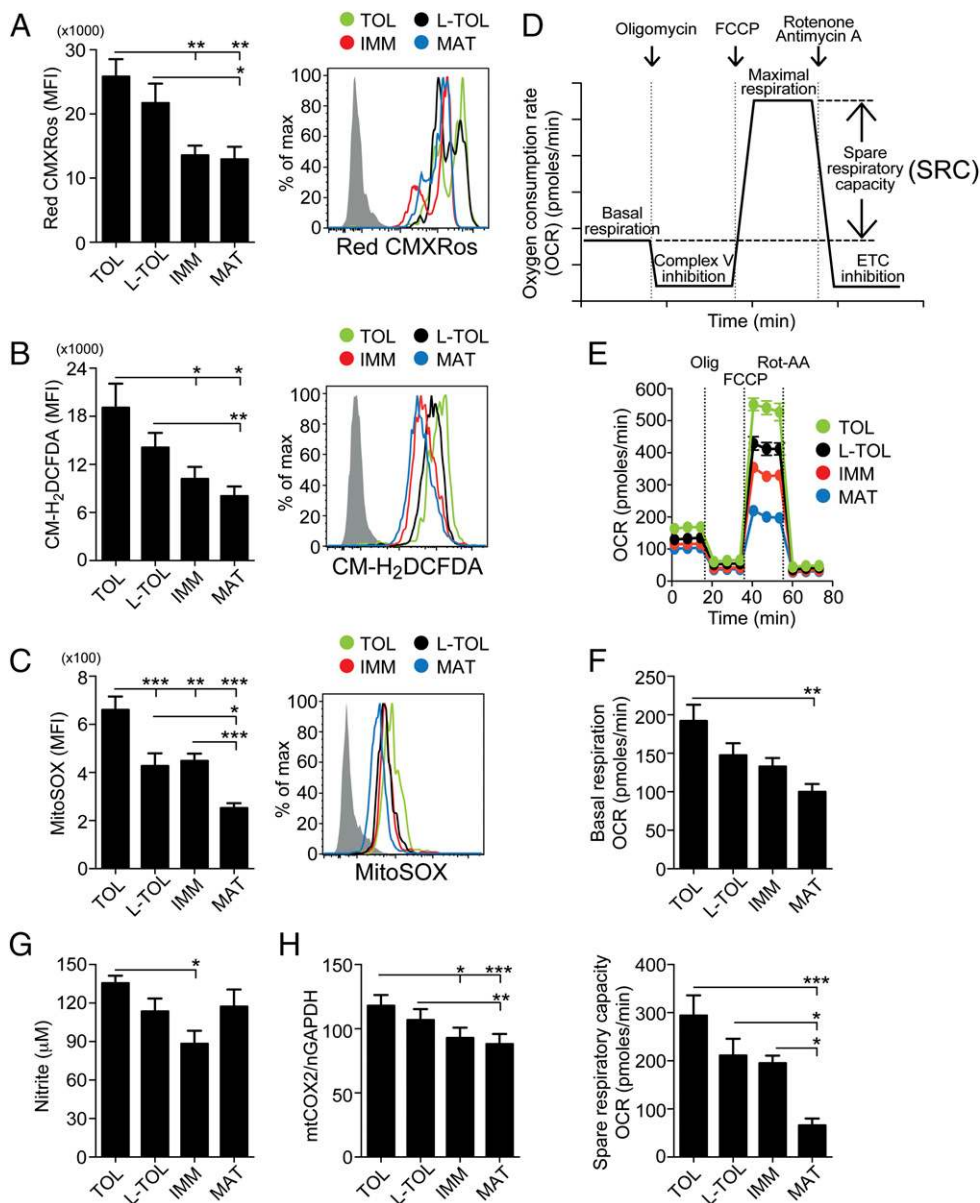
FIGURE 3. Characterization of mitochondrial function from tolerogenic to immunogenic moDCs. (**A–C**, *left*) Mitochondrial membrane potential (MitoTracker Red CMXRos) (A), ROS (CM-H$_2$DCFDA) (B), and SO (MitoSOX) (C) levels in moDCs obtained by flow cytometric analysis. The data of four independent experiments were pooled. Mean ± SEM. *Right*, Representative flow cytometry histogram of each bar shows tolerogenic (TOL, green), LPS-tolerogenic (L-TOL, black), immature (IMM, red), and mature (MAT, blue) moDCs. Unlabeled control moDCs in gray. (**D**) Schematic representation of a real-time mitochondrial respiration. OCR analysis starting from basal respiration and after the addition of oligomycin (complex V inhibition), FCCP (maximal respiration induction), and rotenone/antimycin A mixture (electron transport chain [ETC] inhibition). The mitochondrial SRC (maximal subtracted from basal respiration) is derived from the OCR curve. (**E**) Representative kinetic study of mitochondria OCR (mpH/min) in tolerogenic (green), LPS-tolerogenic (black), immature (red), and mature (blue) moDCs by using sequential addition of oligomycin (Olig), FCCP, and rotenone/antimycin A (Rot-AA). (**F**, *upper* and *lower panels*) OCR quantification of basal respiration and SRC of moDCs, respectively. The data were pooled from five independent experiments. Mean ± SEM. (**G**) NO as nitrite levels was measured in supernatants from moDC cultures. Data were pooled from 12 independent experiments. Mean ± SEM. (**H**) Mitochondria mass determination as the ratio mitochondrial (mt) DNA/nuclear (n) DNA, mtCOX2/nGAPDH. The data were pooled from five independent experiments. Mean ± SEM. All statistical differences were analyzed by one-way ANOVA with a Tukey multiple comparison posttest. *$p < 0.05$, **$p < 0.01$, ***$p < 0.001$. MFI, mean fluorescence intensity.

moDCs. Moreover, mitochondrial FAO activity was the highest in tolerogenic and immature moDCs, whereas LPS-induced maturation has a negative impact on this pathway.

moDC maturation increases glycolytic rate but decreases glycolytic capacity and reserve

In addition to FAO, another important energy source for OXPHOS is glycolysis. Similar to our previous FAO analysis, we found that tolerogenic and mature moDCs have differential expressions of

glycolytic genes (Fig. 5A). Surprisingly, most glycolytic genes were increased in tolerogenic moDCs relative to mature moDCs. Furthermore, tolerogenic and LPS-tolerogenic moDCs demonstrated an increase in glycolytic enzyme protein content, specifically in lactate dehydrogenase B (LDHB) (Fig. 5B). The protein content of a number of other glycolytic enzymes among moDC types did not differ (Supplemental Fig. 3B). Because lactic acid and protons are released from cells during glycolysis (20, 21), we analyzed the glycolytic activity of moDCs by measuring lactate

FIGURE 4. Gene expression, protein content, and functional characterization of FAO in moDCs. (**A**) Heat map of gene level *z*-score normalized gene expression levels of FAO components in all moDC types (IMM, immature; L-TOL, LPS-tolerogenic; MAT, mature moDCs; TOL, tolerogenic). (**B**) Protein content of enzymes ACADM, HADHA/HADHB, carnitine palmitoyltransferase 2 (CPT2), and EHHADH in moDCs. The data of five to eight independent experiments were pooled; mean ± SEM. (**C**) Representative kinetic study of mitochondria OCR (mpH/min) in tolerogenic (green), LPS-tolerogenic (black), immature (red), and mature (blue) moDCs using sequential addition of either etomoxir (Eto) or media, oligomycin (Olig), FCCP, and rotenone/antimycin A (Rot-AA). (**D**) Bars show the level of FAO activity (FAO index) in moDCs. The data were poled from four independent experiments. Mean ± SEM. (**E**) Fatty acid uptake in moDCs. The level of fluorescent fatty acid uptake was measured in moDCs as relative fluorescent units (RFU). The data were pooled from five independent experiments. Mean ± SEM. All statistical differences were analyzed by one-way ANOVA with a Tukey multiple comparison posttest. $*p < 0.05$, $**p < 0.01$.
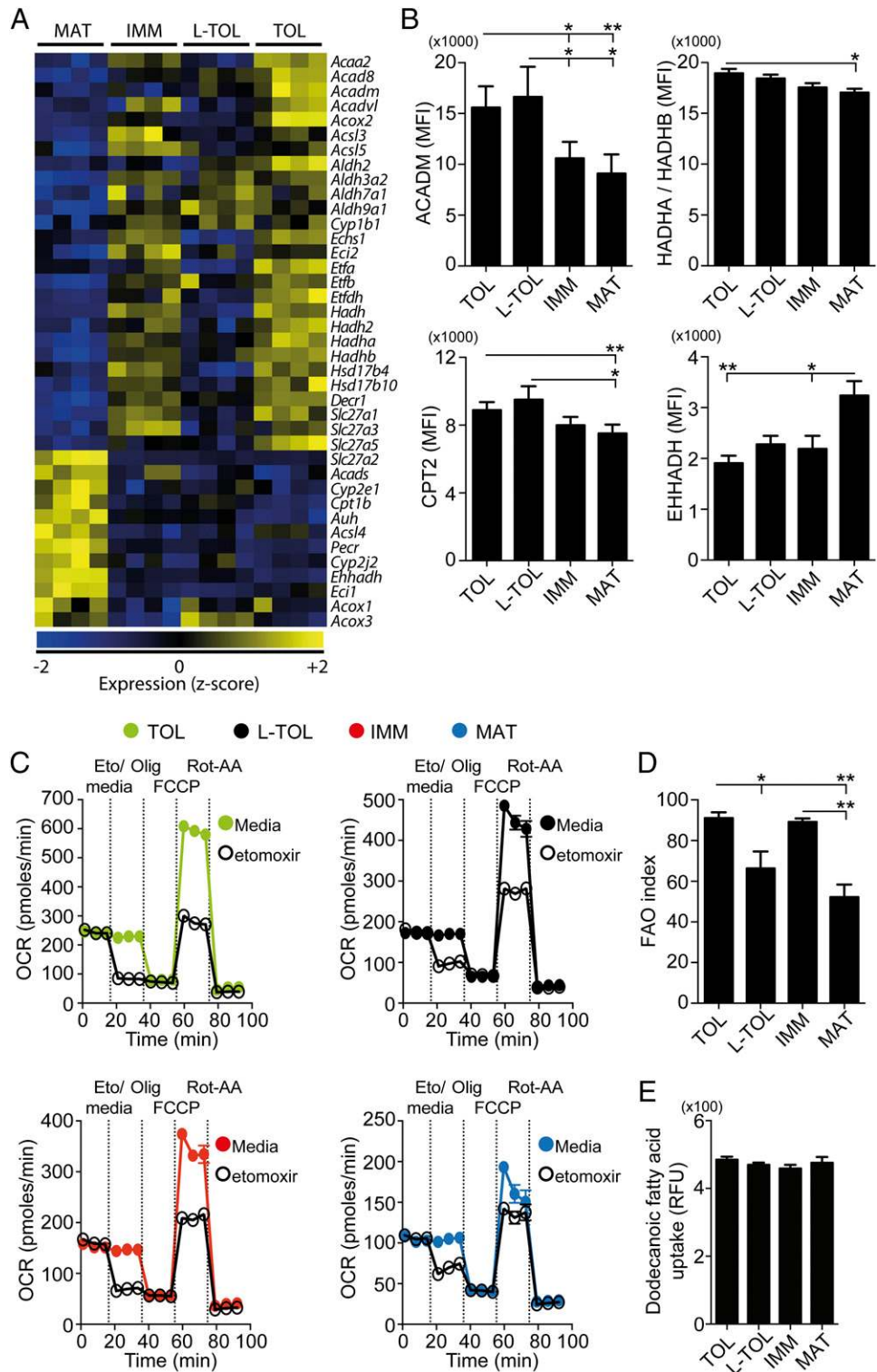
from moDC culture supernatants and by performing a real-time analysis of ECAR. Lactate production by mature moDCs was higher than immature moDCs, but not compared with tolerogenic moDCs (Fig. 5C). Despite this difference in lactate production between mature and immature moDCs, we observed no measurable difference in glucose uptake among all moDC types (Fig. 5D). The schematic real-time analysis in moDCs glycolysis using a Seahorse bioanalyzer is depicted in Fig. 5E. Real-time analysis of glycolysis showed that tolerogenic and immature moDCs exhibited a higher maximal glycolysis (induced by oligomycin in

presence of glucose; Fig. 5F) compared with LPS-treated moDCs (Fig. 5F). Quantitative analysis showed no significant differences during the basal stage among moDCs (Fig. 5G, *left panel*). Because the basal stage has the potential to accumulate other nonglycolytic extracellular acidification sources, for example, carbonic acid (20, 21), ECAR values were normalized (basal ECAR subtraction) to determine the corrected ECAR values for glycolytic rate and glycolytic capacity. In the presence of glucose, the glycolytic rate of all moDCs increased compared with the basal stage, with mature moDCs exhibiting a higher glycolytic
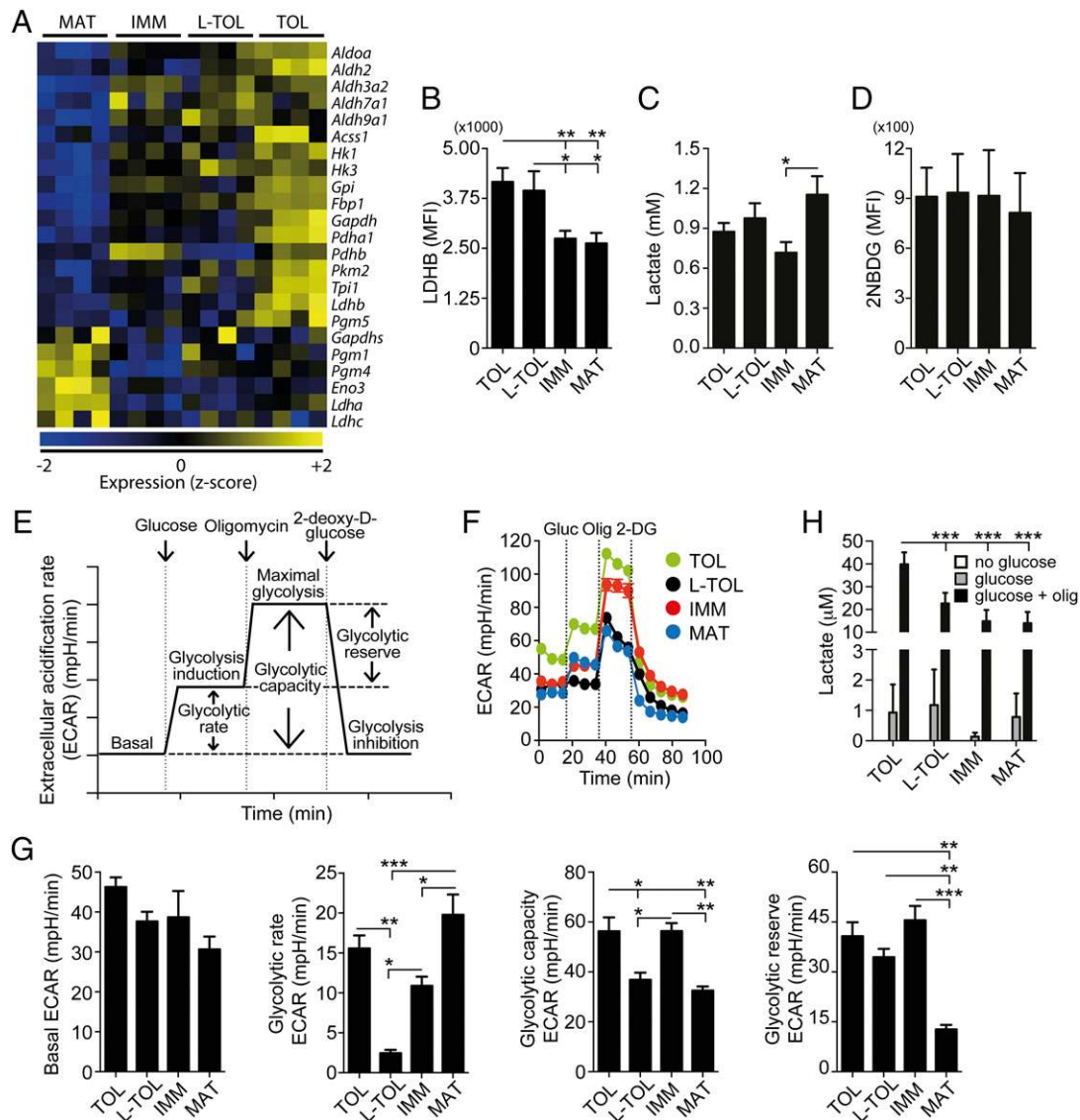
FIGURE 5. Gene expression, protein content, and functional characterization of glycolysis in moDCs. (**A**) Heat map shows gene level *z*-score–normalized glycolysis gene expression levels in all moDC types (IMM, immature; L-TOL, LPS-tolerogenic; MAT, mature moDCs; TOL, tolerogenic). (**B**) Protein content of enzyme LDHB in moDCs. The data were pooled from eight independent experiments. Mean $\pm$ SEM. (**C**) Lactate content from moDC supernatants cultures at day 7. The data were pooled from 12 independent experiments. Mean $\pm$ SEM. (**D**) 2-(*N*-(7-nitrobenz-2-oxa-1,3-diazol-4-yl)amino)-2-deoxyglucose (2NBDG) uptake study in moDCs. The levels of the fluorescent deoxyglucose uptake by moDCs were measured by flow cytometry (mean fluorescence intensity [MFI]). The data were poled from five independent experiments. Mean $\pm$ SEM. (**E**) Schematic representation of real-time glycolysis. ECAR analysis starts from basal ECAR, in which the cells were incubated in glucose-free media followed by the addition of glucose (glycolysis induction), olygomycin (which induces maximal cell glycolysis and complex V inhibition), and finally 2-deoxy-D-glucose (glycolysis inhibition). Glycolytic rate (glycolysis induction subtracted for basal ECAR), glycolytic capacity (maximal glycolysis subtracted for basal ECAR), and glycolytic reserve (maximal glycolysis subtracted for glycolysis induction) are derived from the ECAR curve. (**F**) Representative kinetic study of glycolysis-dependent ECAR (mpH/min) in tolerogenic (TOL, green), LPS-tolerogenic (L-TOL, black), immature (IMM, red), and mature (MAT, blue) moDCs by using sequential addition of glucose (Gluc), oligomycin (Olig), and 2-DG. (**G**) Bars show basal ECAR levels (*left*), glycolytic rate (*middle left*), glycolytic capacity (*middle right*), and glycolytic reserve (*right*) of moDCs. The data were pooled from three independent experiments; mean $\pm$ SEM. Statistical differences were analyzed by one-way ANOVA with a Tukey multiple comparison posttest. (**H**) Lactate content from cultured moDCs supernatants under no glucose (white), glucose, and glucose in the presence of oligomycin (Olig) media for 75 min. The data were pooled from five independent experiments. Mean $\pm$ SEM. Statistical differences were analyzed by two-way ANOVA with a Tukey multiple comparison posttest. $*p < 0.05$, $**p < 0.01$, $***p < 0.001$.

rate than immature moDCs (Fig. 5G, *left middle panel*). No significant differences were found between mature and tolerogenic moDCs (Fig. 5G, *left middle panel*). The glycolytic capacity of tolerogenic and immature moDCs was higher than mature moDCs (Fig. 5G, *right middle panel*). Finally, in contrast to their high glycolytic rate, glycolytic reserve was the lowest in mature moDCs (Fig. 5G, *right panel*). The high glycolytic capacity of tolerogenic moDCs was also observed in terms of lactate production (Fig. 5H). In summary, we observed a differential expression

of glycolytic genes in tolerogenic and mature moDCs. Functional analysis of glycolytic energetics demonstrated that tolerogenic moDCs have a higher glycolytic capacity and reserve, despite mature moDCs shift to glycolysis.

FAO activity is important for maintaining immune tolerogenic state

An important discovery in the field of immunometabolism showed that modulating metabolic pathways also modulates immunoge-

nicity of murine BMDCs (9–11). We therefore wanted to address whether modulation of metabolic pathways could affect the tolerogenicity and immunogenicity of human moDCs. Along this line, we used different metabolic modulators on LPS-tolerogenic moDCs to evaluate how these compounds might impair the so-called "resistance to maturation" of these cells (also referred to as "persistent state of immaturity") (13, 22, 23) and, additionally, how the metabolic modulation could affect immunogenicity of mature moDCs.

Consistent with previous reports in murine BMDCs (10, 11), inhibitors of glycolysis decreased the phenotypic maturation of LPS-activated mature moDCs. In more detail, MHC class II levels were inhibited in the presence of oxamate (LDH inhibitor) (Fig. 6A, *upper left panel*), as were the levels of CD80 surface expression (Fig. 6A, *upper right panel*). CD86 levels were reduced in the presence of 2-DG (Fig. 6A, *lower left panel*), whereas expression of CD83 demonstrated a tendency to decrease in the presence of both glycolysis inhibitors (Fig. 6A, *lower right panel*). Strikingly, unlike mature moDCs, LPS-tolerogenic moDCs showed an increase in MHC class II expression in the presence of inhibitors of OXPHOS and FAO (Fig. 6B, *upper left panel*).

We next set out to investigate the effect of metabolic pathway inhibition on tolerogenic function. The direct impact of these metabolic inhibitors on T cell proliferation prohibited their continued presence in the proliferation assays (data not shown). To address their effects on DC immunogenicity, we evaluated the ability of treated and then washed moDCs to stimulate the early activation marker CD69 on 24 h allogeneic CD4$^+$ T cell cocultures. Consistent with its impact on MHC class II expression, inhibition of FAO on LPS-tolerogenic moDCs led to a small but significant increase in responder CD4$^+$ T cell activation (Fig. 6C), indicating that FAO observed in these cells is required for their tolerogenic function. Treatment with oligomycin leads to significant T cell death regardless of the moDC type used (data not shown). Globally, these data suggest that the observed phenotypic changes of surface maturation in metabolically modulated LPS-tolerogenic moDCs were coincident with allogeneic CD4$^+$ T cell activation.

LPS-induced maturation decreases the bioenergetic adaptation capacity of moDCs

Thus far, these data have demonstrated a pronounced metabolic difference between the different moDCs, in terms of OXPHOS, FAO, and glycolysis, and we therefore investigated how the interplay of these metabolic pathways maintain and adapt to the energy requirements of moDCs.

We first analyzed the total ATP content in moDCs. Results demonstrated that despite having the lowest level of mitochondrial OXPHOS and an equivalent glycolytic rate to tolerogenic moDCs, mature moDCs produced the highest levels of ATP (Fig. 7A). Inhibition of OXPHOS using oligomycin led to a modest reduction of ATP content in tolerogenic and immature moDCs (Fig. 7B). Following FAO inhibition with etomoxir, we observed that ATP content decreased in all moDC types, although this drop was more significant in mature moDCs (Fig. 7C). Inhibition of glycolysis using 2-DG did not show observable differences in ATP content reduction between mature moDCs and tolerogenic moDCs (Fig. 7D). In all cases, these observations were not a consequence of cell death (Supplemental Fig. 4A), even after using combinations of OXPHOS, FAO, and glycolysis inhibition, which depleted almost all ATP content (Supplemental Fig. 4B) with no observable effect on cell viability (Supplemental Fig. 4C). In conclusion, these data suggested that tolerogenic and immature moDCs show a bioenergetic plasticity for intracellular ATP supply, which is forfeited following LPS stimulation
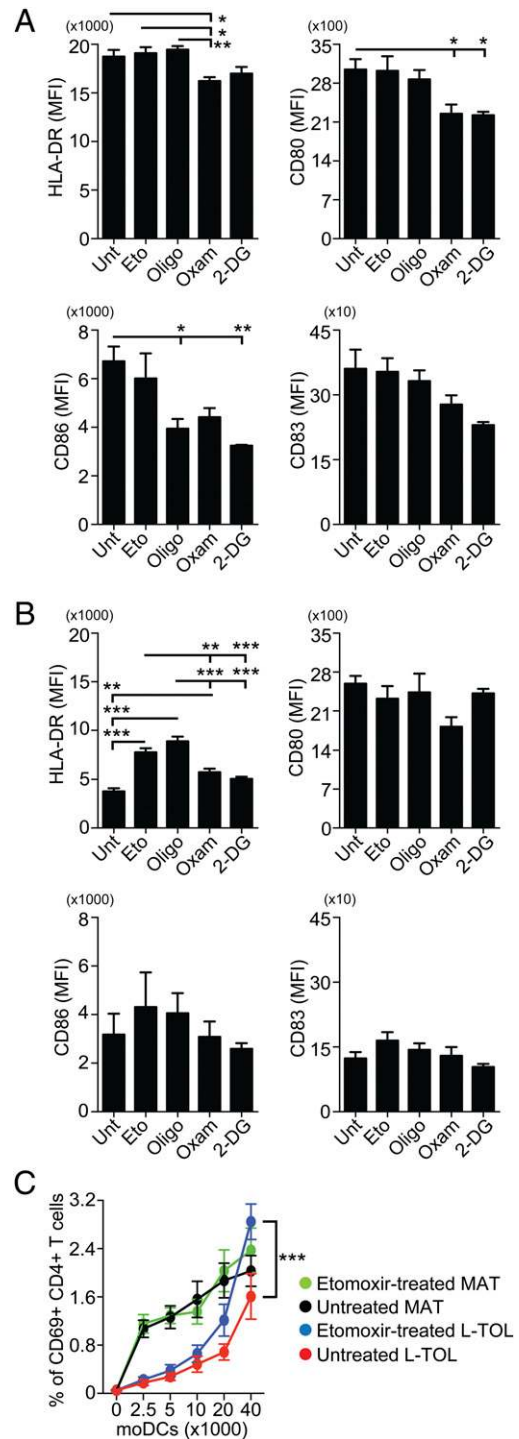

FIGURE 6. Effect of metabolic modulators on mature and LPS-tolerogenic moDCs. Surface expression analysis of HLA-DR (MHC class II), CD80, CD86, and CD83 in metabolically modulated mature (**A**) and LPS-tolerogenic (**B**) moDCs by flow cytometry. Dexamethasone/vitamin D$_3$–treated and untreated moDCs were treated with the metabolic modulators etomoxir (Eto), oligomycin (Olig), oxamate (Oxam), 2-DG, or left untreated (Unt) followed by 24 h LPS stimulation. The data were pooled from six independent experiments; mean ± SEM. Statistical differences were analyzed by one-way ANOVA with a Tukey multiple comparison posttest. (**C**) Early activation of allogeneic CD4 T cells induced by etomoxir-treated or untreated mature (MAT) and LPS-tolerogenic (L-TOL) moDCs assessed by surface expression analysis of CD69. The data were pooled from four independent experiments; mean ± SEM. Statistical differences were analyzed by two-way ANOVA with a Tukey multiple comparison posttest. *$p < 0.05$, **$p < 0.01$, ***$p < 0.001$.
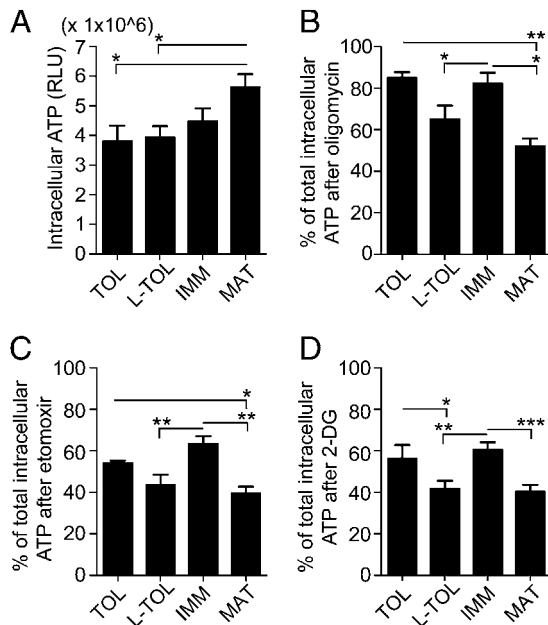
FIGURE 7. Bioenergetic adaptation of moDCs after inhibition of catabolic pathways. (**A**) Total intracellular ATP content in moDCs (IMM, immature; L-TOL, LPS-tolerogenic; MAT, mature; TOL, tolerogenic). ATP percentage of total after moDCs treatment with oligomycin (**B**), etomoxir (**C**), and 2-DG (**D**). The data were pooled from five independent experiments. Mean $\pm$ SEM. Statistical differences were analyzed by one-way ANOVA with a Tukey multiple comparison posttest. *$p < 0.05$, **$p < 0.01$, ***$p < 0.001$.

Discussion

We characterized the state of energetic metabolism in human moDC types across a spectrum of immunogenicity, using protein and gene expression analysis as well as functional metabolic assays. At the transcriptomic level, we determined that tolerogenic and immature moDCs displayed a pronounced catabolic program manifested by OXPHOS, FAO, and glycolysis, whereas mature moDCs had a predominant proinflammatory program. Additionally, mitochondrial respiration, ROS, and SO production, as well as mitochondrial SRC, were detected at high, intermediate, and low levels in tolerogenic, immature, and mature moDCs, respectively. We demonstrate that the level of OXPHOS activity negatively correlates with immunogenicity.

Despite that both vitamin D_3 and dexamethasone alone have been reported to induce a tolerogenic effect on moDCs (23), we chose the combination of these compounds because this approach provides more potent tolerogenic effect than when individual drugs are used (14). This is currently an accepted model of human tolerogenic DC generation with a therapeutic utility (24). Because of the above-mentioned reasons, we used this pharmacologic approach to obtain potent tolerogenic moDCs to study their metabolism.

The moDC types differ in their utilization of fatty acids for metabolism. The degree of FAO was the same in tolerogenic and immature moDCs. LPS-stimulated moDCs had a lower FAO index relative to tolerogenic and immature moDCs, consistent with observations in murine mature BMDCs (11). Interestingly, our analyses demonstrated that tolerogenic and immature moDCs preferentially expressed FAO genes associated with the mitochondria, in contrast to mature moDCs, which expressed peroxisomal FAO genes. Earlier studies have reported that moDC maturation by LPS induces release of arachidonic acid (25, 26), which is in part catabolized by peroxisomal FAO (27–29).

Therefore, it is tempting to speculate that moDC maturation, which is paralleled by a decrease in mitochondrial FAO activity, leads to an increase in peroxisomal FAO activity. However, the functional role of peroxisomal FAO in moDC immunogenicity remains to be determined.

The LPS-induced switch from OXPHOS to glycolysis under aerobic conditions (Warburg effect) has been described for the process of murine BMDC maturation and was similar to our findings. In this sense, we have shown metabolic differences between immature and mature moDCs. Mature moDCs have lower mitochondrial SRC (Fig. 3E, 3F) and FAO index (Fig. 4C, 4D) as well as higher glycolytic rate (Fig. 5G), which is mirrored by higher lactate production (Fig. 5C). In murine BMDCs, a similar phenomenon has been described during maturation: increased glycolytic rate, increased lactate production, and relative decrease in OXPHOS/FAO compared with glycolysis (11). However, whereas in murine BMDCs this switch leads to a complete blockade of the mitochondrial respiration (OXPHOS) (9), our data suggest that in human moDCs the switch of OXPHOS to glycolysis is more "balanced." This is supported by our observation that in human moDCs, metabolic modulators could affect the mitochondrial respiration, OXPHOS, and FAO in mature moDCs (Figs. 3E, 3F, 4D) and is in stark contrast to what has been observed in mature BMDCs, in which mitochondrial respiration is completely refractory to metabolic modulators (9). This limited but persistent OXPHOS (Fig. 3E, 3F) and FAO activity (Fig. 4C, 4D) in mature moDCs is still able to provide ~40% of ATP under glycolysis inhibition (Fig. 7D), in contrast to what has been described in mature murine BMDCs, in which >90% of their ATP production depends on glycolysis. In other words, murine BMDCs are able to provide only 10% of ATP under glycolysis inhibition (9). Additionally, because mature BMDCs are almost absolutely dependent on glycolysis for ATP, the replacement of glucose by galactose has shown a detrimental effect on their viability (9). This is in contrast to what we have observed in human mature moDCs, which after 24 h of incubation with 50 mM 2-DG only showed a decrease in viability of a maximum of 15–20% (data not shown), which means that mature moDCs maintain some level of energetic plasticity for surviving. Interestingly, the switch from OXPHOS to glycolysis appears to be different between murine DC populations. Splenic DC populations such as CD4$^+$ DCs and CD8α$^+$ DCs stimulated ex vivo with LPS did not induce the switch of OXPHOS to glycolysis (9) compared with murine inflammatory moDCs. In conclusion, our data suggest a switch from OXPHOS to glycolysis during moDC maturation, which is balanced compared with the striking switch observed during the maturation of murine BMDCs. Finally, the evidence suggests that the switch from OXPHOS to glycolysis during maturation may be cell type specific.

From our ATP content analysis, catabolic pathways other than OXPHOS, FAO, and glycolysis can be analyzed as a whole. The coinhibition of glycolysis and OXPHOS as well as the coinhibition of glycolysis and FAO declined the ATP production by >90% (Supplemental Fig. 4B). Considering that these experiments were performed in DMEM media supplemented with glucose, pyruvate, and L-glutamine (OCR medium), the <10% of ATP remnant reveals that the ATP production may originate from the TCA cycle. Despite this minor amount of ATP compared with the compensatory amount of ATP produced under the inhibition of OXPHOS, FAO, or glycolysis (Fig. 7), the TCA cycle probably has an important role in anabolic processes, for instance, during DC maturation (30).

Another striking metabolic difference between murine BMDCs and human moDCs is the role of NO in the inhibition of mito-

chondrial respiration. The mechanism of inhibition of mitochondrial respiration in murine mature BMDCs has been shown to be mediated by NO (9). During the maturation of murine BMDCs, the transcription of inducible NO synthase (iNOS, *NOS2*) increases and the enzyme starts producing NO, which in turn inhibits mitochondrial respiration (9). Our transcriptomic analyses of human moDCs have revealed that iNOS expression in all moDC types is not significantly different (data not shown). Interestingly, the levels of neuronal NO synthase (*NOS3*) were the highest in tolerogenic moDCs (data not shown). Taken together, iNOS appears to be an important isoform expressed in murine BMDCs, but not in human moDCs. Nonetheless, we analyzed the NO production in moDCs and we found that tolerogenic moDCs showed significantly higher NO content than did immature moDCs (Fig. 3G). Most importantly, we did not find differences in NO production between mature moDCs and immature moDCs (Fig. 3G) despite their different mitochondrial activity. Thus, our data suggest that the decreased mitochondrial spare respiratory capacity observed in mature moDCs is NO independent.

The finding that tolerogenic and immature moDCs showed higher glycolytic capacity and reserve than did mature moDCs was rather surprising. This suggests that tolerogenic and immature moDCs still maintain well-structured glycolytic machinery under aerobic conditions (Figs. 5G, 5H, 7B). Thus, compared with mature moDCs, tolerogenic and immature moDCs display a higher spare metabolic capacity and plasticity, which can be triggered under OXPHOS restriction.

Although, tolerogenic moDCs had the highest OXPHOS activity, they did not demonstrate high ATP production, nor did they show an ability to recover ATP content during inhibition of glycolysis (Fig. 7A, 7D). These observations indicate that the increased mitochondrial activity in tolerogenic moDCs may be committed to maintaining a high output of ROS. This is supported by gene expression data, which indicate a state of mitochondrial dysfunction (Fig. 1A, 1B). Moreover, it has been described that dexamethasone-treated muscle cells increase the rate of non–phosphorylative oxygen consumption (31) and that vitamin D_3 increases ROS production (32), which may suggest less efficient ATP production from OXPHOS. Interestingly, tolerogenic moDCs were more affected by etomoxir than oligomycin in terms of ATP production. This phenomenon has been previously reported (33, 34). Based on the study of Pike et al. (33), etomoxir may have a central inhibitory role on TCA, probably influencing the depletion of NADPH content, that leads to a depletion of the antioxidant system, which in turn promotes oxidative stress that affects the compensatory increase in glycolysis. In synthesis, the role of intracellular redox balance in regulating the differentiation and function of tolerogenic moDCs has yet to be determined. Importantly, note that a number of transcription factors are highly sensitive to nuclear redox state, including NF-κB and AP-1 (35).

Although inhibition of FAO and OXPHOS in tolerogenic moDCs led to an increase in phenotypic markers of maturation, this was accompanied by a modest increase in T cell stimulatory function. We speculate two possible scenarios: 1) the phenotypic changes induced by the metabolic modulators may not have been sufficient to induce a functionally immunogenic boost effect on LPS-tolerogenic moDCs, or 2) the observed phenotypic changes could be kept as long as the moDCs stay in the presence of metabolic modulators. Future research should focus on the transience of metabolic modulation on moDC function and consider genetic silencing/enhancing methods to permanently modulate specific metabolic pathways

In conclusion, we show that tolerogenic moDCs have a defined metabolic phenotype characterized by a prominent mitochondrial OXPHOS and high glycolytic capacity. Importantly, we observed that LPS-induced maturation decreases the metabolic plasticity, which could provide new insights into how metabolic adaptations of tolerogenic/immunogenic moDCs may affect the outcome of immune responses in vivo.

References

1. Steinman, R. M., D. Hawiger, and M. C. Nussenzweig. 2003. Tolerogenic dendritic cells. *Annu. Rev. Immunol.* 21: 685–711.
2. Tisch, R. 2010. Immunogenic versus tolerogenic dendritic cells: a matter of maturation. *Int. Rev. Immunol.* 29: 111–118.
3. Joffre, O. P., E. Segura, A. Savina, and S. Amigorena. 2012. Cross-presentation by dendritic cells. *Nat. Rev. Immunol.* 12: 557–569.
4. Takeuchi, O., and S. Akira. 2010. Pattern recognition receptors and inflammation. *Cell* 140: 805–820.
5. Vicente-Manzanares, M., and F. Sánchez-Madrid. 2004. Role of the cytoskeleton during leukocyte responses. *Nat. Rev. Immunol.* 4: 110–122.
6. Pearce, E. L., and E. J. Pearce. 2013. Metabolic pathways in immune cell activation and quiescence. *Immunity* 38: 633–643.
7. Sukumar, M., J. Liu, Y. Ji, M. Subramanian, J. G. Crompton, Z. Yu, R. Roychoudhuri, D. C. Palmer, P. Muranski, E. D. Karoly, et al. 2013. Inhibiting glycolytic metabolism enhances CD8+ T cell memory and antitumor function. *J. Clin. Invest.* 123: 4479–4488.
8. van der Windt, G. J., and E. L. Pearce. 2012. Metabolic switching and fuel choice during T-cell differentiation and memory development. *Immunol. Rev.* 249: 27–42.
9. Everts, B., E. Amiel, G. J. van der Windt, T. C. Freitas, R. Chott, K. E. Yarasheski, E. L. Pearce, and E. J. Pearce. 2012. Commitment to glycolysis sustains survival of NO-producing inflammatory dendritic cells. *Blood* 120: 1422–1431.
10. Jantsch, J., D. Chakravortty, N. Turza, A. T. Prechtel, B. Buchholz, R. G. Gerlach, M. Volke, J. Gläsner, C. Warnecke, M. S. Wiesener, et al. 2008. Hypoxia and hypoxia-inducible factor-1α modulate lipopolysaccharide-induced dendritic cell activation and function. *J. Immunol.* 180: 4697–4705.
11. Krawczyk, C. M., T. Holowka, J. Sun, J. Blagih, E. Amiel, R. J. DeBerardinis, J. R. Cross, E. Jung, C. B. Thompson, R. G. Jones, and E. J. Pearce. 2010. Toll-like receptor-induced changes in glycolytic metabolism regulate dendritic cell activation. *Blood* 115: 4742–4749.
12. Jin, P., T. H. Han, J. Ren, S. Saunders, E. Wang, F. M. Marincola, and D. F. Stroncek. 2010. Molecular signatures of maturing dendritic cells: implications for testing the quality of dendritic cell therapies. *J. Transl. Med.* 8: 4.
13. Morelli, A. E., and A. W. Thomson. 2007. Tolerogenic dendritic cells and the quest for transplant tolerance. *Nat. Rev. Immunol.* 7: 610–621.
14. Ferreira, G. B., F. S. Kleijwegt, E. Waelkens, K. Lage, T. Nikolic, D. A. Hansen, C. T. Workman, B. O. Roep, L. Overbergh, and C. Mathieu. 2012. Differential protein pathways in 1,25-dihydroxyvitamin D_3 and dexamethasone modulated tolerogenic human dendritic cells. *J. Proteome Res.* 11: 941–971.
15. Guo, W., L. Jiang, S. Bhasin, S. M. Khan, and R. H. Swerdlow. 2009. DNA extraction procedures meaningfully influence qPCR-based mtDNA copy number determination. *Mitochondrion* 9: 261–265.
16. Smyth, G. K. 2004. Linear models and empirical bayes methods for assessing differential expression in microarray experiments. *Stat. Appl. Genet. Mol. Biol.* 3: Article3.
17. Chu, C. C., N. Ali, P. Karagiannis, P. Di Meglio, A. Skowera, L. Napolitano, G. Barinaga, K. Grys, E. Sharif-Paghaleh, S. N. Karagiannis, et al. 2012. Resident CD141 (BDCA3)+ dendritic cells in human skin produce IL-10 and induce regulatory T cells that suppress skin inflammation. *J. Exp. Med.* 209: 935–945.
18. Wang, Y., A. W. Mohsen, S. J. Mihalik, E. S. Goetzman, and J. Vockley. 2010. Evidence for physical association of mitochondrial fatty acid oxidation and oxidative phosphorylation complexes. *J. Biol. Chem.* 285: 29834–29841.
19. Grynberg, A., and L. Demaison. 1996. Fatty acid oxidation in the heart. *J. Cardiovasc. Pharmacol.* 28(Suppl 1): S11–S17.
20. Gatenby, R. A., and R. J. Gillies. 2004. Why do cancers have high aerobic glycolysis? *Nat. Rev. Cancer* 4: 891–899.
21. Kato, Y., S. Ozawa, C. Miyamoto, Y. Maehata, A. Suzuki, T. Maeda, and Y. Baba. 2013. Acidic extracellular microenvironment and cancer. *Cancer Cell Int.* 13: 89.
22. Griffin, M. D., W. Lutz, V. A. Phan, L. A. Bachman, D. J. McKean, and R. Kumar. 2001. Dendritic cell modulation by 1α,25 dihydroxyvitamin D_3 and its analogs: a vitamin D receptor-dependent pathway that promotes a persistent

state of immaturity in vitro and in vivo. *Proc. Natl. Acad. Sci. USA* 98: 6800–6805.

23. Maldonado, R. A., and U. H. von Andrian. 2010. How tolerogenic dendritic cells induce regulatory T cells. *Adv. Immunol.* 108: 111–165.

24. Hilkens, C. M., and J. D. Isaacs. 2013. Tolerogenic dendritic cell therapy for rheumatoid arthritis: where are we now? *Clin. Exp. Immunol.* 172: 148–157.

25. Harizi, H., M. Juzan, V. Pitard, J. F. Moreau, and N. Gualde. 2002. Cyclooxygenase-2-issued prostaglandin E$_2$ enhances the production of endogenous IL-10, which down-regulates dendritic cell functions. *J. Immunol.* 168: 2255–2263.

26. Valera, I., N. Fernández, A. G. Trinidad, S. Alonso, G. D. Brown, A. Alonso, and M. S. Crespo. 2008. Costimulation of dectin-1 and DC-SIGN triggers the arachidonic acid cascade in human monocyte-derived dendritic cells. *J. Immunol.* 180: 5727–5736.

27. Hiltunen, J. K., T. Kärki, I. E. Hassinen, and H. Osmundsen. 1986. Beta-oxidation of polyunsaturated fatty acids by rat liver peroxisomes. A role for 2,4-dienoyl-coenzyme A reductase in peroxisomal beta-oxidation. *J. Biol. Chem.* 261: 16484–16493.

28. Ricciotti, E., and G. A. FitzGerald. 2011. Prostaglandins and inflammation. *Arterioscler. Thromb. Vasc. Biol.* 31: 986–1000.

29. Williard, D. E., T. L. Kaduce, S. D. Harmon, and A. A. Spector. 1998. Conversion of eicosapentaenoic acid to chain-shortened omega-3 fatty acid metabolites by peroxisomal oxidation. *J. Lipid Res.* 39: 978–986.

30. Everts, B., E. Amiel, S. C. Huang, A. M. Smith, C. H. Chang, W. Y. Lam, V. Redmann, T. C. Freitas, J. Blagih, G. J. van der Windt, et al. 2014. TLR-driven early glycolytic reprogramming via the kinases TBK1-IKKε supports the anabolic demands of dendritic cell activation. *Nat. Immunol.* 15: 323–332.

31. Dumas, J. F., G. Simard, D. Roussel, O. Douay, F. Foussard, Y. Malthiery, and P. Ritz. 2003. Mitochondrial energy metabolism in a model of undernutrition induced by dexamethasone. *Br. J. Nutr.* 90: 969–977.

32. Somjen, D., S. Katzburg, M. Grafi-Cohen, E. Knoll, O. Sharon, and G. H. Posner. 2011. Vitamin D metabolites and analogs induce lipoxygenase mRNA expression and activity as well as reactive oxygen species (ROS) production in human bone cell line. *J. Steroid Biochem. Mol. Biol.* 123: 85–89.

33. Pike, L. S., A. L. Smift, N. J. Croteau, D. A. Ferrick, and M. Wu. 2011. Inhibition of fatty acid oxidation by etomoxir impairs NADPH production and increases reactive oxygen species resulting in ATP depletion and cell death in human glioblastoma cells. *Biochim. Biophys. Acta* 1807: 726–734.

34. de Moura, M. B., R. Uppala, Y. Zhang, B. Van Houten, and E. S. Goetzman. 2014. Overexpression of mitochondrial sirtuins alters glycolysis and mitochondrial function in HEK293 cells. *PLoS ONE* 9: e106028. Available at: http://journals.plos.org/plosone/article?id=10.1371/journal.pone.0106028.

35. Schenk, H., M. Klein, W. Erdbrügger, W. Dröge, and K. Schulze-Osthoff. 1994. Distinct effects of thioredoxin and antioxidants on the activation of transcription factors NF-κB and AP-1. *Proc. Natl. Acad. Sci. USA* 91: 1672–1676.